



Metasurface-Enabled Remote Quantum Interference

Pankaj K. Jha,¹ Xingjie Ni,¹ Chihhui Wu,¹ Yuan Wang,¹ and Xiang Zhang^{1,2,*}

¹*NSF Nanoscale Science and Engineering Center (NSEC), 3112 Etcheverry Hall, University of California, Berkeley, California 94720, USA*

²*Materials Science Division, Lawrence Berkeley National Laboratory, 1 Cyclotron Road, Berkeley, California 94720, USA*

(Received 11 February 2015; published 6 July 2015)

An anisotropic quantum vacuum (AQV) opens novel pathways for controlling light-matter interaction in quantum optics, condensed matter physics, etc. Here, we theoretically demonstrate a strong AQV over macroscopic distances enabled by a judiciously designed array of subwavelength-scale nanoantennas—a metasurface. We harness the phase-control ability and the polarization-dependent response of the metasurface to achieve strong anisotropy in the decay rate of a quantum emitter located over distances of hundreds of wavelengths. Such an AQV induces quantum interference among radiative decay channels in an atom with orthogonal transitions. Quantum vacuum engineering with metasurfaces holds promise for exploring new paradigms of long-range light-matter interaction for atom optics, solid-state quantum optics, quantum information processing, etc.

DOI: [10.1103/PhysRevLett.115.025501](https://doi.org/10.1103/PhysRevLett.115.025501)

PACS numbers: 81.05.Xj, 73.20.Mf, 81.16.Nd

Quantum interference (QI) arises from the indistinguishable paths of photons. QI in spontaneous emission, from nearly degenerate excited states in a multilevel quantum emitter, leads to a variety of remarkable effects such as coherent population trapping [1], an efficient quantum photoengine [2], etc. In an isotropic quantum vacuum, QI has a stringent requirement of nonorthogonal transition dipole moments which is rarely met in atomic systems [3–5]. However, by breaking the isotropic nature of the quantum vacuum, one can circumvent such a constraint and achieve QI for orthogonal transitions [6]. For instance, it has been theoretically proposed that an atom in the vicinity of few tens of nanometers of a metallic surface [7,8] or embedded in a photonic crystal [9], may experience an anisotropic quantum vacuum (AQV). Unfortunately in these approaches, both precise positioning [10–12] and optically addressing the atom for quantum applications are challenging in experiments due to near surface interactions such as surface thermal noise, Casimir-Polder force, quenching, and so forth. A strong AQV over remote distances from any material interface is, therefore, imperative but has never been realistically possible [13,14].

In this Letter, we propose and theoretically demonstrate a long-sought-after solution for experimentally observable QI in atoms over remote distances using an engineered surface—a metasurface. We harness the phase-control ability and the polarization-dependent response of a judiciously designed metasurface to tailor the quantum vacuum and induce strong anisotropy for an atom at a macroscopic distance over $100\lambda_0$, where λ_0 is the wavelength in free space. Quantum vacuum engineering with metasurfaces creates unprecedented opportunities for long-range interactions between quantum emitters, solid-state quantum optics, spintronics, and the decoherence-free subspace for quantum information transfer.

A quantum emitter, in the vicinity of a metallic interface [15], can strongly interfere with its own spontaneously emitted photon after reflecting from the surface, and display intriguing interference effects [16–18]. For instance, one can design and construct an interface, near which, a quantum emitter displays orientation dependent decay rate which is a manifestation of an AQV [19]. With multilevel quantum emitters, such an AQV can induce QI among radiative decay channels even if the corresponding dipole moments are orthogonal to each other. One of the most straightforward ways to engineer the quantum vacuum is to place an infinite-size perfect metallic surface (parallel to the $x - y$ plane) in the vicinity ($d \ll \lambda_0$) of an x dipole. This metallic interface forms an out-of-phase image of the x dipole. The destructive interference between the direct emission and the reflected field results in the suppression of the spontaneous emission. However, this suppression is quickly washed out beyond $d \sim \lambda_0$ due the fading interference between the direct and the reflected fields. By symmetry, the same mirror can also form an out-of-phase image of a y dipole. This symmetry leads to an isotropic quantum vacuum in the $x - y$ plane parallel to the mirror. On the other hand, by integrating the metasurface we can break this in-plane symmetry and induce strong interference even when the quantum emitter is at a macroscopic distance.

Metasurfaces have attracted great interest due to their exceptional light-manipulation properties [20–22]. Recent studies have shown that metasurfaces provide a higher degree of freedom in molding the flow of light, compared to bulk metamaterials [21]. It can be used to bend the light abnormally in a fairly broad wavelength range [23,24], enhance optical spin-orbit interaction [25,26], couple efficiently propagating waves and surface waves [27], create planar optical lenses [28], build ultrathin holograms [29], enhance nonlinear optical responses in semiconductor heterostructures [30], perform mathematical operations

[31], negative refraction and planar focusing [32]. However, most of the applications to date have mainly focused on classical fields where the average number of photons per mode is large ($n \gg 1$). Here, we show that a prudentially designed metasurface can also be harnessed for *nonclassical* fields, for instance, a single photon field, and enable QI in a multilevel quantum emitter.

It is advantageous to use a metasurface for quantum vacuum engineering. First, a metasurface offers a greater degree of freedom in shaping a polarization dependent wave front of the fields [21]. Second, the incident and reflected fields propagate through an optically thin layer of subwavelength-scale nanoantennas, the absorption loss due to a metal is minimal and a strong backaction on the quantum emitter can be realized. Third, optically thin and planar structure of the metasurface makes it a promising candidate for micro-optical devices like atom chips [33], to explore long range interaction between trapped atoms, ions, quantum dots, etc.

The schematic illustration of the metasurface-enabled remote AQV is shown in Fig. 1. The metasurface breaks the symmetry of quantum vacuum fluctuations and creates a strong AQV in the vicinity of a distant quantum emitter. This anisotropy manifests itself in the angular dependence of the decay rate of a two-level quantum emitter with the transition dipole moment parallel to the surface (x - y plane). In general the decay of a two-level quantum emitter, dipole moment in the x - y plane, is given by $\gamma = \gamma_{xx} \cos^2(\varphi) + \gamma_{yy} \sin^2(\varphi)$ where φ is the azimuthal angle. In an isotropic quantum

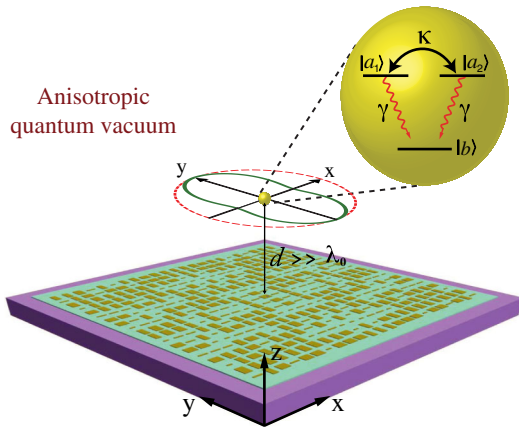


FIG. 1 (color online). Metasurface-enabled macroscopic quantum vacuum engineering. The metasurface creates a strong AQV in the vicinity of a quantum emitter at some macroscopic distance d . Decay of an in-plane, linear dipole is anisotropic (solid green curve) with respect to an isotropic quantum vacuum with no physical boundary (dashed red line). The inset shows a three-level atom, at some macroscopic distance from the metasurface, with coupled orthogonal transitions ($\varphi_{a_1 b} \cdot \varphi_{a_2 b}^* = 0$) whose coupling strength κ depends on the anisotropy of the quantum vacuum. Coherent coupling among the transitions is accomplished by exchanging *virtual photons* via the quantum vacuum. Such an AQV induces QI among the radiative decay channels.

vacuum with no physical boundary, the decay of this dipole is isotropic (red dashed line), i.e., independent of its orientation φ , but in the presence of a metasurface (green solid line) the decay is anisotropic. Such an AQV induces QI among the decay channels in a multilevel quantum emitter.

Nanoantennas, which resonate with the incident light, can shift the phase through their resonances for the scattered light. By changing their resonance properties, e.g., shifting the resonant frequency, through the nano-antenna designs, we can effectively control the amount of the phase shifted in the scattered light. It can be intuitively understood as the light being held for some time due to the resonance before it gets reemitted, which gives a finite phase delay. An array of such subwavelength-scale nanoantennas, namely a metasurface, collaboratively can mold the wave front of the scattered light into an arbitrary form. Without loss of generality, we distributed the nanoantennas on a surface in such a way that it acts as a spherical-mirror for an x dipole while simultaneously serving as a normal mirror for a y dipole. Polarization dependent response of the metasurface is illustrated in Fig. 2(a) where the x -polarized light is reflected back to the source while the y - z -polarized light is defocused. In Fig. 2(b) we have plotted the spatial intensity distribution of a dipole located at $3.7 \mu\text{m}$ from the metasurface with a cross-sectional area of $12 \mu\text{m} \times 12 \mu\text{m}$. Figures 2(c) and 2(d) show the intensity distribution of the reflected field for an x - and

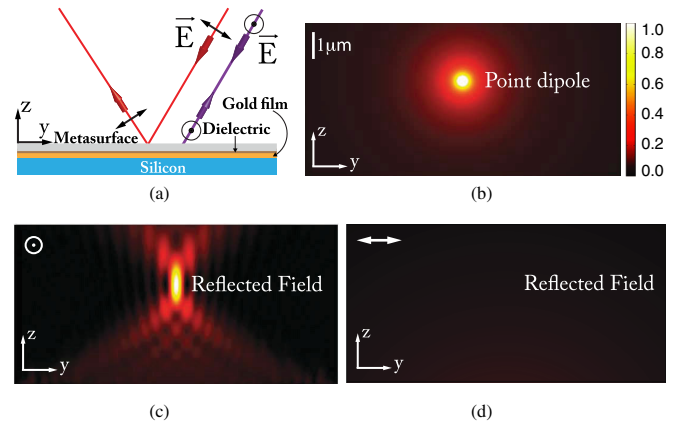


FIG. 2 (color online). Principle of metasurface-enabled remote anisotropic quantum vacuum. (a) Two-dimensional schematic illustration of polarization dependent response of the metasurface. Incident y - z polarized light is defocused by the metasurface while the x -polarized light is focused back to the source. (b) Simulated field intensity distribution from a linear dipole source. (c) Simulated field intensity distribution of the reflected field, above the metasurface, for the x dipole. With an optimized design we achieved 81%, normalized to total field incident on the metasurface, reflection efficiency of the incident field back to the source. However, for the y dipole the incident field is defocused and the corresponding reflected field intensity distribution is shown in (d). For all numerical simulations [(b),(c),(d)] the dipole is located at a distance of $3.7 \mu\text{m}$ from the metasurface with cross-sectional dimension ($12 \mu\text{m} \times 12 \mu\text{m}$).

y -dipole (point) source. One of the limitations of previously studied metasurface designs resides in their poor overall efficiency. This can be overcome with gap plasmon-based gradient metasurfaces by integrating a metallic mirror on the back of the nanoantennas and sandwiching a dielectric spacer layer in between them [34,35]. With the proper optimization tool, we achieved 81% (normalized to the total field incident on the metasurface) in the reflection efficiency for the constitutional nanoantennas of the metasurface for the x polarization through our full-wave numerical simulations (see Supplemental Material [36]). The calculation in this Letter is based on this efficiency.

Polarization selective response can be efficiently achieved by adjusting the phase shifts provided by the constitutional nanoantennas. For x polarization, the required phase shift for a nanoantenna at the coordinate (x_0, y_0) is given by $\phi(x_0, y_0) = \pi + 2k_0\sqrt{r_0^2 + d^2}$, where d is the distance between the quantum emitter and the metasurface, $r_0 = \sqrt{x_0^2 + y_0^2}$, and k_0 is the wave number in the vacuum. The coordinate of the quantum emitter is $(0, 0, d)$. Here we use five different nanoantenna designs of a gold bar as the constitutional elements of the metasurface. Each design provides a distinct phase shift for the x polarization but not the same phase shift for the y polarization through its anisotropic plasmonic resonances. The designs with required phase shifts are obtained by sweeping over different geometrical parameters, the length and the width of the gold bars, using full-wave finite element simulations. The five designed nanoantennas are shown in Fig. 3(a). When the size [namely, l_x and l_y as shown in the left panel of Fig. 3(a)] of the nanoantenna changes, the phase shift of the scattered light of the nanoantenna will change accordingly in the x -polarized incidence. The response of the five nanoantennas covers the phase shift from 0 to 2π and matches well with the ideal phase shifts required by the constituent nanoantennas such that the necessary spherical phase profile is imprinted by the metasurface. In Fig. 3(b) we have plotted two-dimensional distribution of the phase profile required upon the reflection to focus the incident light and compensate the optical path length from an x dipole to its image, where the height and the color of the surface plot indicates the phase shift.

Figure 4 shows the calculated radiative decay rate of a two-level quantum emitter above an infinite-sized metasurface versus the distance d/λ_0 . The decay rate is obtained by utilizing the ratio between numerically calculated total emitted power from a dipole [42] with and without the presence of a metasurface. For the x dipole a constant decay rate $\gamma_{xx} \sim 0.6\gamma_0$ can be engineered, while for a y dipole the decay rate oscillates [42] and quickly goes to the value of $\gamma_{yy} = \gamma_0$ and remains constant thereafter. Thus we can achieve an AQV regardless of the distance by optimizing the design for each point along the z axis. The upper limit to the distance between the quantum emitter and the metasurface is fundamentally constrained by the photonic coherence length

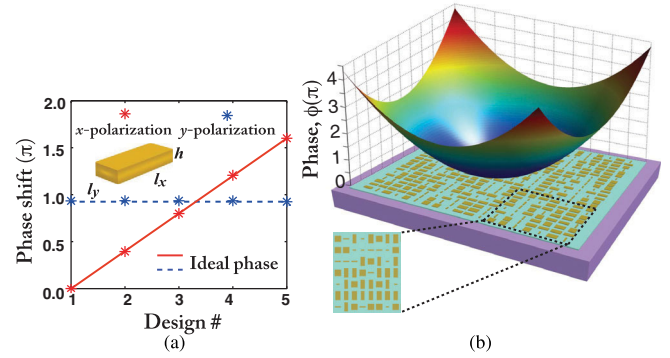


FIG. 3 (color online). Polarization dependent phase shift and vanishing optical path: (a) Phase shift imprinted by the five constitutional nanoantennas for the x -polarized (red stars) and y -polarized (blue stars) incident light. For the x -polarized light the response is linear and covers the full phase range 0 to 2π , and matches well with the required ideal phase indicated by the solid red line, while for the y -polarized light the corresponding phase shift for each constitutional nanoantenna is a constant. (b) Two-dimensional distribution of the phase profile required upon the reflection to focus the incident light and compensate the optical path length from an x dipole to its image. The inset shows the top view of a small piece. The dimensions (l_x nm, l_y nm, 30 nm) of the five nanoantennas are: (32, 154), (144, 161), (166, 159), (186, 157), and (229, 153), respectively.

[14]. For a given design, considering the metasurface as a focusing device which is diffraction limited, the position tolerance for the dipole is on the order of a wavelength. An infinitely large metasurface is equivalent to a solid angle of 2π in the perspective of the dipole. Practically, the solid angle can be close to 2π if the metasurface is sufficiently large. For example, for the solid angle of 1.998π , if the dipole is at a distance of $100\lambda_0$, the radius of the metasurface is about $2234\lambda_0$, and the resulting $\gamma_{xx} = 0.62\gamma_0$. If we consider ^{133}Cs as an isolated trapped atom at $100\lambda_0$, where $\lambda_0 = 894$ nm (D_1 transition) the radius of the metasurface to project 1.998π radian of the solid angle is ~ 2 mm.

To see the effect of an AQV on a multilevel quantum emitter we will consider a three-level atom in V configuration, as shown in Fig. 1 (inset). The details of the atomic transitions and equation of motion are given in the Supplemental Material [36]. In an AQV the orthogonal transitions ($|a_{1,2}\rangle \rightarrow |b\rangle$) are coupled whose strength is quantified by the cross damping [6] term $\kappa \sim \wp_{a_1b} \cdot \Im m[\vec{G}(\mathbf{r}_0, \mathbf{r}_0, \omega_{ab})] \cdot \wp_{a_2b}^*$ where \mathbf{r}_0 is the position vector of the atom, ω_{ab} is the atomic transition frequency and $\Im m[\vec{G}]$ is the imaginary part of the dyadic Green's function. In terms of the local coordinates the cross damping term takes the form $\kappa = (\gamma_{xx} - \gamma_{yy})/2$. From Fig. (4) we obtain $\gamma_{xx} = 0.6, \gamma_{yy} = 1$ which yields $\kappa = -0.2$. If we consider $d = 20\lambda_0$ where $\lambda_0 = 894$ nm, we obtain a significant cross damping at a distance of $\sim 18 \mu\text{m}$ from the metasurface. It is worth mentioning that by introducing another metasurface above the quantum

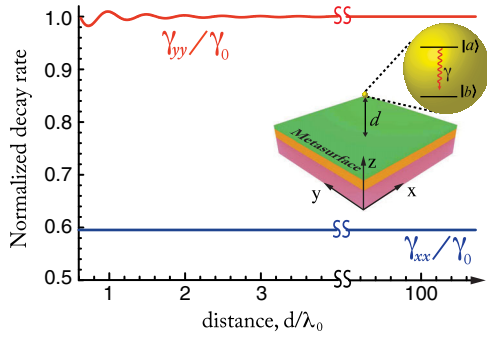
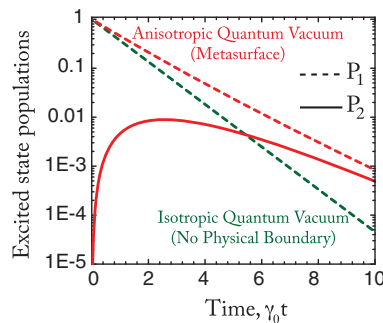


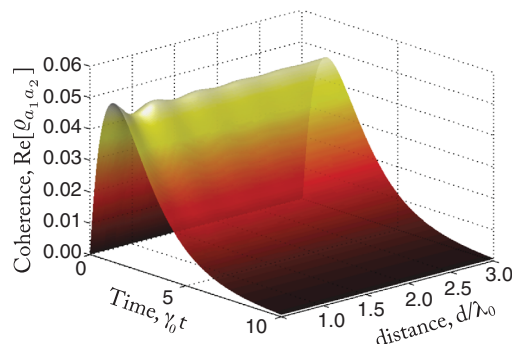
FIG. 4 (color online). Anisotropic decay rate of a quantum emitter over remote distances. Plot of the normalized decay rate of an x dipole (blue line) and y dipole (red line) located at the focus of the metasurface against distance d/λ_0 . As the distance between the x dipole and the metasurface is increased (along the z direction) the decay rate does not change and remains flat. However, for the y dipole the decay rate oscillates and quickly goes to the value of $\gamma_{yy} = \gamma_0$ and remains constant thereafter. We can induce an AQV in the x - y plane, i.e., $\gamma_{xx} \neq \gamma_{yy}$ over remote distances by designing the metasurface for each point along the z axis.

emitter, the decay rate can be further reduced and the anisotropy can be enhanced. On the other hand with plasmonic, negative-index metamaterials (with losses), or above a photonic crystal the cross damping $\kappa \sim 0$ over such distances.

In Fig. 5(a) we have plotted the population of the excited states $|a_{1,2}\rangle$ as a function of normalized time $\gamma_0 t$ (see Supplemental Material for calculations [36]). In an isotropic quantum vacuum with no physical boundary the atom decays exponentially with a characteristic time constant $\tau_c = \gamma_0^{-1}$ (dashed green) and the population of the state $|a_2\rangle$ remains zero. On the other hand, when the atom is located at the focus of the metasurface, it experiences an AQV which induces quantum interference among the decay channels $|a_{1,2}\rangle \rightarrow |b\rangle$.



(a)



(b)

FIG. 5 (color online). Anisotropic quantum vacuum-induced quantum interference: (a) Plot of the excited state populations $P_i = q_{a_i a_i}$ of a three-level atom (shown in Fig. 1 inset) located at $20\lambda_0$ distance from the metasurface, initially prepared in $|a_1\rangle$, as a function of normalized time $\gamma_0 t$. In an isotropic quantum vacuum, with no physical boundary ($\kappa = 0$) the atom decays exponentially (dashed green) with time constant γ_0^{-1} and the population of the state $|a_2\rangle$ remains zero. On the other hand, when the atom is located at the focus of the metasurface the decay of the excited state $|a_1\rangle$ is suppressed (dashed red) and a nonzero population transfers to the level $|a_2\rangle$ (solid red). (b) 3D plot of the transient coherence ($\text{Re}[q_{a_1 a_2}]$) between the excited states as a function of normalized time ($\gamma_0 t$) and distance (d/λ_0). Nonzero coherence, a clear signature of vacuum-induced cross damping, can be sustained over macroscopic distances.

Subsequently, the decay of the excited state $|a_1\rangle$ is suppressed (dashed red) and we see nonzero population transfer to $|a_2\rangle$ (solid red). At initial times, the evolution of the population of the state $|a_2\rangle$ is $q_{a_2 a_2}(t) \approx (|\kappa_1|^2/4)t^2$ while the coherence grows linearly as $q_{a_1 a_2} \approx (\kappa_1^*/2)t$. In Fig. 5(b) we have plotted the transient coherence (real part of $q_{a_1 a_2}$) at different points in space along the z axis. Nonzero coherence, along with nonzero population in the state $|a_2\rangle$, is a clear signature of vacuum-induced cross damping between the two transitions $|a_{1,2}\rangle \leftrightarrow |b\rangle$. Vacuum induced coherence effects can also be probed by studying resonance profiles [43], photon-photon correlation [44], etc.

A viable way to place and hold quantum emitters at remote distances from the plasmonic metasurface is by trapping ultracold atomic gases in optical lattices or atomic chips. For instance, trapping a Bose-Einstein condensate (BEC) at $\sim 5 \mu\text{m}$ from a gold wire has been successfully demonstrated in Ref. [45]. By contrast, trapping below or at submicron distances from a metallic interface is often challenging owing to fluctuating spatial and temporal magnetic fields, surface tunneling, Casimir-Polder forces, thermal noise, etc. [10]. The possibility of trapping an ultra-cold atom at submicron dimensions near a wire has been proposed in Ref. [46]. However, although metallic interfaces can induce strong anisotropic quantum vacuum at distances $d \ll \lambda_0$, precise control over positioning and holding atoms within this limit is extremely difficult if not impossible. Hence, creating a strong AQV at distances $d \gg \lambda_0$ is indeed necessary for viable experimental demonstrations. We anticipate that our approach will not only bridge the gap between plasmonic metasurfaces and QED [47] but also open a door for quantum engineering of light-matter interactions with single or no photons, constructing a long-range interaction between quantum emitters, and exploring fundamental quantum physics.

The authors acknowledge funding support from the Multidisciplinary University Research Initiative from the Air Force Office of Scientific Research (AFOSR MURI Award No. FA9550-12-1-0488). P. K. J. conceived the idea, performed the atomic analytical and numerical calculations. X. N. designed the metasurface, conducted numerical simulations and decay rate calculations. X. Z. and Y. W. guided the research. All authors contributed to discussions and wrote the Letter.

P. K. J. and X. N. contributed equally to this work.

*To whom all correspondence should be addressed.
xiang@berkeley.edu

- [1] G. S. Agarwal, *Quantum Statistical Theories of Spontaneous Emission and Their Relation to Other Approaches*, Springer Tracts in Modern Physics: Quantum Optics Vol. 70, edited by G. Mohler *et al.* (Springer-Verlag, Berlin, 1974).
- [2] M. O. Scully, K. R. Chapin, K. E. Dorfman, M. B. Kim, and A. Svidzinsky, *Proc. Natl. Acad. Sci. U.S.A.* **108**, 15097 (2011).
- [3] H.-R. Xia, C. Y. Ye, and S.-Y. Zhu, *Phys. Rev. Lett.* **77**, 1032 (1996).
- [4] M. V. G. Dutt, J. Cheng, B. Li, X. Xu, X. Li, P. R. Berman, D. G. Steel, A. S. Bracker, D. Gammon, S. E. Economou, R.-B. Liu, and L. J. Sham, *Phys. Rev. Lett.* **94**, 227403 (2005).
- [5] K. P. Heeg, H.-C. Wille, K. Schlage, T. Guryeva, D. Schumacher, I. Uschmann, K. S. Schulze, B. Marx, T. Kampf, G. G. Paulus, R. Rohlsberger, and J. Evers, *Phys. Rev. Lett.* **111**, 073601 (2013).
- [6] G. S. Agarwal, *Phys. Rev. Lett.* **84**, 5500 (2000).
- [7] V. Yannopoulos, E. Paspalakis, and N. V. Vitanov, *Phys. Rev. Lett.* **103**, 063602 (2009).
- [8] Y. Gu, L. Wang, P. Ren, J. Zhang, T. Zhang, O. J. Martin, and Q. Gong, *Nano Lett.* **12**, 2488 (2012).
- [9] G.-X. Li, F.-L. Li, and S.-Y. Zhu, *Phys. Rev. A* **64**, 013819 (2001).
- [10] *Atom Chips*, edited by J. Reichel and V. Vuletic (Wiley-VCH, Weinheim, Germany, 2011).
- [11] D. E. Chang, A. S. Sorensen, P. R. Hemmer, and M. D. Lukin, *Phys. Rev. Lett.* **97**, 053002 (2006).
- [12] D. E. Chang, J. D. Thompson, H. Park, V. Vuletic, A. S. Zibrov, P. Zoller, and M. D. Lukin, *Phys. Rev. Lett.* **103**, 123004 (2009).
- [13] Y. Yang, J. Xu, H. Chen, and S.-Y. Zhu, *Phys. Rev. Lett.* **100**, 043601 (2008).
- [14] J. Kastel and M. Fleischhauer, *Phys. Rev. A* **71**, 011804(R) (2005).
- [15] A. Delga, J. Feist, J. Bravo-Abad, and F. J. Garcia-Vidal, *Phys. Rev. Lett.* **112**, 253601 (2014).
- [16] K. E. Dorfman, P. K. Jha, D. V. Voronine, P. Genevet, F. Capasso, and M. O. Scully, *Phys. Rev. Lett.* **111**, 043601 (2013).
- [17] P. K. Jha, X. Yin, and X. Zhang, *Appl. Phys. Lett.* **102**, 091111 (2013).
- [18] G. S. Agarwal and S.-A. Biehs, *Opt. Lett.* **38**, 4421 (2013).
- [19] P. W. Milonni, *The Quantum Vacuum: An Introduction to Quantum Electrodynamics* (Academic Press, New York, 1994).
- [20] A. V. Kildishev, A. Boltasseva, and V. M. Shalaev, *Science* **339**, 1232009 (2013).
- [21] N. Yu and F. Capasso, *Nat. Mater.* **13**, 139 (2014).
- [22] N. Fang, H. Lee, C. Sun, and X. Zhang, *Science* **308**, 534 (2005).
- [23] N. Yu, P. Genevet, M. A. Kats, F. Aieta, J.-P. Tetienne, F. Capasso, and Z. Gaburro, *Science* **334**, 333 (2011).
- [24] X. Ni, N. K. Emani, A. V. Kildishev, A. Boltasseva, and V. M. Shalaev, *Science* **335**, 427 (2012).
- [25] N. Shitrit, I. Yulevich, E. Maguid, D. Ozeri, D. Veksler, V. Kleiner, and E. Hasman, *Science* **340**, 724 (2013).
- [26] X. Yin, Z. Ye, J. Rho, Y. Wang, and X. Zhang, *Science* **339**, 1405 (2013).
- [27] S. Sun, Q. He, S. Xiao, Q. Xu, X. Li, and L. Zhou, *Nat. Mater.* **11**, 426 (2012).
- [28] F. Aieta, P. Genevet, M. A. Kats, N. Yu, R. Blanchard, Z. Gaburro, and F. Capasso, *Nano Lett.* **12**, 4932 (2012).
- [29] X. Ni, A. V. Kildishev, and V. M. Shalaev, *Nat. Commun.* **4**, 2807 (2013).
- [30] J. Lee, M. Tymchenko, C. Argyropoulos, P. Y. Chen, F. Lu, F. Demmerle, G. Boehm, M. C. Amann, A. Alu, and M. Belkin, *Nature (London)* **511**, 65 (2014).
- [31] A. Silva, F. Monticone, G. Castaldi, V. Galdi, A. Alu, and N. Engheta, *Science* **343**, 160 (2014).
- [32] R. Fleury, D. L. Sounas, and A. Alu, *Phys. Rev. Lett.* **113**, 023903 (2014).
- [33] R. Folman, P. Krüger, J. Schmiedmayer, J. Denschlag, and C. Henkel, *Adv. At. Mol. Opt. Phys.* **48**, 263 (2002).
- [34] S. Sun, K.-Y. Yang, C.-M. Wang, T.-K. Juan, W. T. Chen, C. Y. Liao, Q. He, S. Xiao, W.-T. Kung, and G.-Y. Guo, *Nano Lett.* **12**, 6223 (2012).
- [35] A. Pors, O. Albrektsen, I. P. Radko, and S. I. Bozhevolnyi, *Sci. Rep.* **3**, 2155 (2013).
- [36] See Supplemental Material at <http://link.aps.org/supplemental/10.1103/PhysRevLett.115.025501> for details of the equation of motion of the quantum emitter (three-level atom in *V* configuration) and calculation of reflection efficiency. It also includes Refs. [37–41].
- [37] P. B. Johnson and R. W. Christy, *Phys. Rev. B* **6**, 4370 (1972).
- [38] D. A. Cardimona, M. G. Raymer, and C. R. Stroud Jr., *J. Phys. B* **15**, 55 (1982).
- [39] P. Zhou and S. Swain, *Phys. Rev. Lett.*, **78**, 3995 (1997).
- [40] H. T. Dung, S. Y. Buhmann, L. Knoll, D.-G. Welsch, S. Scheel, and J. Kastel, *Phys. Rev. A* **68**, 043816 (2003).
- [41] G. S. Agarwal and A. K. Patnaik, *Phys. Rev. A* **63**, 043805 (2001).
- [42] L. Novotny and B. Hecht, *Principles of Nano-Optics* (Cambridge University Press, Cambridge, England, 2006).
- [43] K. E. Dorfman, P. K. Jha, and S. Das, *Phys. Rev. A* **84**, 053803 (2011).
- [44] S. Das and G. S. Agarwal, *Phys. Rev. A* **77**, 033850 (2008).
- [45] S. Wildermuth, S. Hofferberth, I. Lesanovsky, E. Haller, L. M. Andersson, S. Groth, I. Bar-Joseph, and P. Krüger, *Nature (London)* **435**, 440 (2005).
- [46] R. Salem, Y. Japha, J. Chab, B. Hadad, M. Keil, K. A. Milton, and R. Folman, *New J. Phys.* **12**, 023039 (2010).
- [47] J. D. Thompson, T. G. Tiecke, N. P. de Leon, J. Feist, A. V. Akimov, M. Gullans, A. S. Zibrov, V. Vuletic, and M. D. Lukin, *Science* **340**, 1202 (2013).